MIXED MODE FRACTURE CHARACTERIZATION OF ADHESIVE JOINTS

U. Weerts, H. Kossira
Institute of Aircraft Design and Lightweight Structures
Technical University of Braunschweig, Germany

Keywords: *Adhesive, Joint, J-Integral, Mixed-Mode, Fracture*

Abstract

Double Cantilever Beam (DCB) and Single-Lap Joint (SLJ) specimens are investigated with regard to the fracture mechanical behavior on the basis of the J-integral [1].

The J-integral is derived in a formulation, which is useful for a coarse meshed finite element analysis. Therefore, the method bypasses the detailed determination of the strain singularity and the inelastic material behavior at the crack tip. The formulation allows a mixed-mode fracture characterization by simple determinations of the adhesive thickness and near tip adhesive stresses and strains of a continuum mechanics approach. The method is demonstrated by means of a DCB specimen and compared with a physical nonlinear analysis including the crack tip singularity.

Experiments on cyclic loaded DCB and SLJ specimens are analyzed with the above-mentioned theory and indicate the validity of the fracture characterization for the prediction of crack initiation.

1 Introduction

Many fundamentals of the mechanical behavior of bonded joints were pointed out in extensive theoretical and experimental studies. Volkersen [2] determined the adhesive shear stress induced by the axial elongation of the adherends under symmetric load conditions. Goland and Reissner [3] considered the bending deformation of the adherends caused by asymmetric load introduction. The extensive studies of Hart-Smith [4] included the influence of the adhesive shear displacement on the adherend's bending. As the performance of structures and joints grows rapidly, new design methods have been developed paying regard to the fracture mechanics [5], [6]. Most investigations are based on the above-mentioned analytical theories and are used for the determination of fracture properties by means of simple specimens. Fernlund [7] and Fraisse [8] determined fracture parameters on the basis of the Energy Release Rates (ERR) and the J-integral. Both obtained a result with a simple formulation depending on the adhesive thickness and the near tip stress and strain field of a continuum mechanics approach.

In the present paper a general deduction of the method by Fraisse will be shown enabling the use of finite element applications. As the method only requires a coarse mesh, it is qualified for the fracture characterization of complex bondings in thin shell structures.

2 Theoretical Investigations

To obtain generality a tensor notation is used for the derivations [9]. Consequently, a right subscript or superscript characterizes the covariant or contravariant meaning of the symbol; a left superscript indicates the configuration (current = t; initial = 0). Vectors and tensors are written in bold-face type and are distinguished by the context. The summation convention is adopted. The Lagrangian formulation analysis is applied.

2.1 Geometrical relations

Figure 1 shows an adhesively bonded joint in the initial configuration. Any point of the joint can be described by its position vector

$$ {}^{0}\mathbf{x} = {}^{0}x^{i}\, \mathbf{e}_{i} \qquad (1)$$

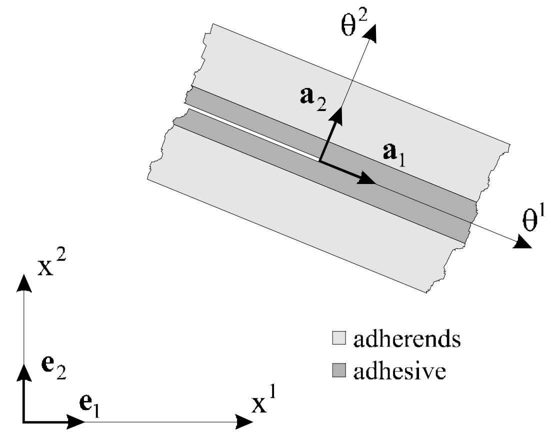

Figure 1: Coordinate systems

with the contravariant components ${}^0x^i$ of the fixed rectangular cartesian system x^i represented by the covariant base vectors $\mathbf{e}_i$. Likewise, the position vector in the current configuration

$$ {}^t\mathbf{x} = {}^tx^i\,\mathbf{e}_i \tag{2}$$

is defined, and the displacement vector is denoted by

$$\mathbf{u} = {}^t\mathbf{x} - {}^0\mathbf{x} = u^i\,\mathbf{e}_i\ . \tag{3}$$

All stress and strain components are associated with the material coordinate system θ^i with the base vectors $\mathbf{a}_i$, which are defined by the total differentials of the position vectors

$$d\,{}^0\mathbf{x} = {}^0\mathbf{x}_{,\theta^i}\,d\theta^i = {}^0\mathbf{a}_i\,d\theta^i\ , \tag{4}$$

$$d\,{}^t\mathbf{x} = {}^t\mathbf{x}_{,\theta^i}\,d\theta^i = {}^t\mathbf{a}_i\,d\theta^i\ , \tag{5}$$

with

$$\frac{\partial(\ )}{\partial\theta^i} = (\ )_{,\theta^i}\ . \tag{6}$$

The material coordinate system is fixed to the joint and orthonormal in the initial configuration. Due to the deformation of the body the system loses its orthonormal character in the current configuration. The deformation of the body in the current configuration may be expressed by the Green-Lagrange strain tensor in the contravariant basis system ${}^0\mathbf{a}^i$ of the initial configuration

$$\boldsymbol{\varepsilon} = \varepsilon_{ij}\ {}^0\mathbf{a}^i\ {}^0\mathbf{a}^j\ , \tag{7}$$

which can be interpreted as the measurement of the difference of the squares of the corresponding line elements of the initial and current configuration

$$ {}^tds^2 - {}^0ds^2 = ({}^ta_{ij} - {}^0a_{ij})\,d\theta^i\,d\theta^j = 2\,\varepsilon_{ij}\,d\theta^i\,d\theta^j\ . \tag{8}$$

${}^0a_{ij}$ and ${}^ta_{ij}$ are the components of the initial and current covariant metric tensor

$$ {}^0a_{ij} = {}^0\mathbf{a}_i\ {}^0\mathbf{a}_j\ , \tag{9}$$

$$ {}^ta_{ij} = {}^t\mathbf{a}_i\ {}^t\mathbf{a}_j\ . \tag{10}$$

The components of the strain tensor can be obtained by equations 3 up to 9

$$\varepsilon_{ij} = \tfrac{1}{2}\left({}^0\mathbf{a}_i\,\mathbf{u}_{,\theta^j} + \mathbf{u}_{,\theta^i}\,{}^0\mathbf{a}_j + \mathbf{u}_{,\theta^i}\,\mathbf{u}_{,\theta^j}\right)\ . \tag{11}$$

Here, a formulation is given in accordance to the evaluation of the J-integral of Rice using scalar products of base vectors and derivatives of the displacement vector. The assumption of small deformations (linear theory), which is applied to the J-integral, gives

$$\varepsilon_{ij} = \tfrac{1}{2}\left({}^0\mathbf{a}_i\,\mathbf{u}_{,\theta^j} + \mathbf{u}_{,\theta^i}\,{}^0\mathbf{a}_j\right)\ . \tag{12}$$

The energetic conjugate second Piola-Kirchhof stress tensor can be determined by the constitutive relations

$$\boldsymbol{\tau} = \mathbf{C}\,\boldsymbol{\varepsilon} = C^{ijkl}\varepsilon_{kl}\ {}^0\mathbf{a}_i\ {}^0\mathbf{a}_j = \tau^{ij}\ {}^0\mathbf{a}_i\ {}^0\mathbf{a}_j\ , \tag{13}$$

where τ^{ij} are the components of the stress tensor in the covariant basis system ${}^0\mathbf{a}_i$ of the initial configuration and C^{ijkl} the elastic coefficients of the body.

2.2 J-Integral

In general, an adhesively bonded joint consists of three components of different mechanical properties, the two adherends and the adhesive. Even if the adherends behave in a linear elastic way, still the viscoplastic material properties of the adhesive must be taken into account considering the validity of the theories.

The application of the J-integral requires a strain-energy density *W*

$$W = \int_0^{\varepsilon} \tau^{ij} d\varepsilon_{ij} \ , \tag{14}$$

which has to be a potential to maintain the path independency of *J*. Summarizing the assumptions the J-integral is only path independent, if the strain is small (see equation (12)) and W is independent of the load history. Using the J-integral as a fracture criterion the strain-rate dependency of the adhesive must be neglected, and the plastic deformations are expected not to control the global deformation behavior of the bonding. Finally, in the case investigated here, the adhesive must behave approximately in a linear elastic way except for the singular crack tip zone. The J-integral of Rice reads

$$J = \int_{\Gamma} (W d\theta^2 - \mathbf{T}\mathbf{u}_{,\theta^1} ds) \ . \tag{15}$$

Here $\mathbf{T}$ is the traction vector defined according to the outward normal $\mathbf{n}$ along Γ, which represents a curve surrounding a crack tip in a contraclockwise sense

$$\mathbf{T} = \boldsymbol{\tau}\mathbf{n} \ . \tag{16}$$

By choosing orthogonal integration paths Γ_{θ^1} in θ^1-direction and Γ_{θ^2} in θ^2-direction, the J-integral can be expressed by

$$J = \int_{\Gamma_{\theta^1}} (\tau^{i2}\ {}^0\mathbf{a}_i \mathbf{u}_{,\theta^1}) d\theta^1 + \int_{\Gamma_{\theta^2}} (\tfrac{1}{2}\tau^{ij}\varepsilon_{ij} - \tau^{i1}\ {}^0\mathbf{a}_i \mathbf{u}_{,\theta^1}) d\theta^2 \ , \tag{17}$$

where a linear elastic behavior is adopted. The stress tensor does not depend on the θ^3-direction

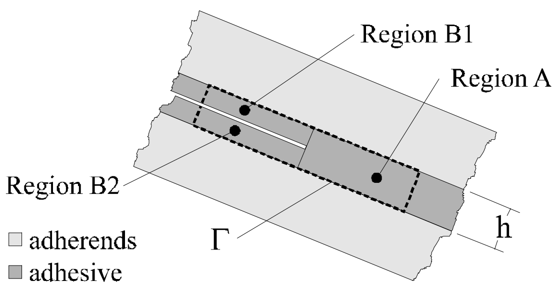

Figure 2: Integration path within the adhesive

considering the two-dimensional stress state and thus, τ^{13} and τ^{23} are zero. With equation (12) and the assumption of plain stress $\tau^{33} = 0$ or plain strain $\varepsilon_{33} = 0$ the integral can be written as

$$J = \int_{\Gamma_{\theta^1}} (\tau^{i2}\ {}^0\mathbf{a}_i \mathbf{u}_{,\theta^1}) d\theta^1 + \tfrac{1}{2}\int_{\Gamma_{\theta^2}} (-\tau^{11}\ {}^0\mathbf{a}_1 \mathbf{u}_{,\theta^1} + \tau^{22}\ {}^0\mathbf{a}_2 \mathbf{u}_{,\theta^2} + \tau^{12} ({}^0\mathbf{a}_1 \mathbf{u}_{,\theta^2} - {}^0\mathbf{a}_2 \mathbf{u}_{,\theta^1})) d\theta^2 \ . \tag{18}$$

The bonded structure consists of several materials. Fraisse [8] showed generally that the J-integral is valid, if the interface planes are parallel to the crack surfaces and the propagation direction. In this case, any integration path can be considered inside of the elastic continuum of the joint. In figure 2 a closed path within the adhesive is depicted. The adhesive is divided into the three regions A, B1 and B2. The interference between the regions, especially the singular behavior at the crack tip, is not taken into account, i. e. the stresses and strains are discontinuous but finite at the crack tip boundary of the three regions. The *J*-estimate remains unchanged, if this assumption does not impair the global deformation behavior, which can be shown for specific applications (chapter 2.3).

The stress states of the regions are imposed by their boundary conditions. Due to the small thickness of the adhesive the stress and strain components may be idealized as θ^2-independent. Thus, the stress components τ^{22} and τ^{12} of the regions B1 and B2 are zero in case of no contact at the crack surfaces. As the regions behave in a linear elastic way, it is valid choosing an integration path directly at the crack tip boundary of the three regions with $\theta^1 = 0$

$$J = \tfrac{1}{2}\int_h (-\tau_A^{11}\ {}^0\mathbf{a}_1 \mathbf{u}_{A,\theta^1} + \tau_{B1}^{11}\ {}^0\mathbf{a}_1 \mathbf{u}_{B1,\theta^1} + \tau_{B2}^{11}\ {}^0\mathbf{a}_1 \mathbf{u}_{B2,\theta^1} + \tau_A^{22}\ {}^0\mathbf{a}_2 \mathbf{u}_{A,\theta^2} + \tau_A^{12} ({}^0\mathbf{a}_1 \mathbf{u}_{A,\theta^2} - {}^0\mathbf{a}_2 \mathbf{u}_{A,\theta^1})) d\theta^2 \ , \tag{19}$$

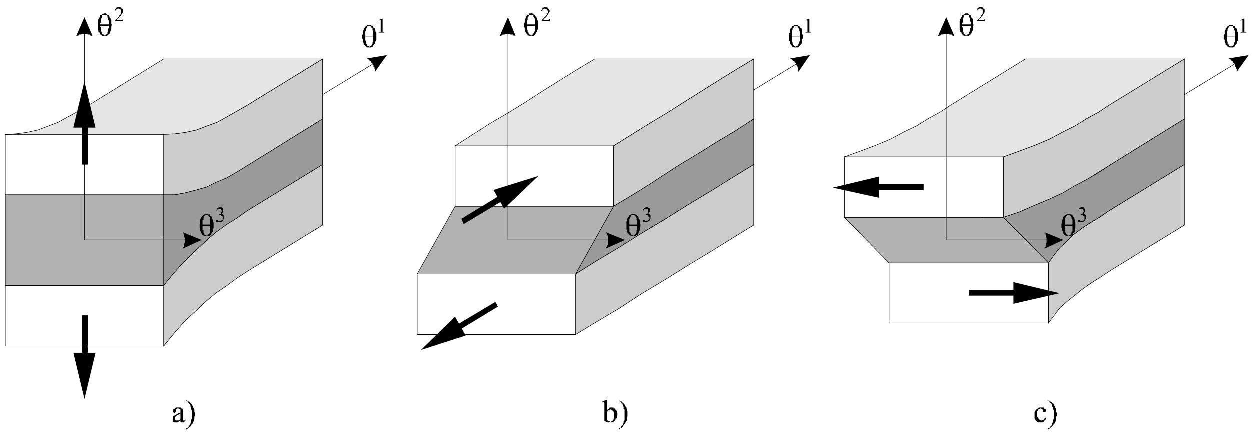

Figure 3: Three basic failure modes for a cracked bonding (crack plane): a) Mode I, opening mode; b) Mode II, sliding mode; c) Mode III, tearing mode

where the right subscripts A, B1 and B2 indicate the region of the applied components at the crack tip and h is the adhesive thickness.

The failure modes can be defined in accordance with the crack closure technique [10], which is based on the energy release rate calculation. Thus, the failure modes are associated with the components of the relative displacements between the adherends at the crack tip, which impose the deformation field on the adhesive (see figure 3). The strain components ${}^{0}\mathbf{a}_2\mathbf{u}_{,\theta^i}$ of the adhesive are determined by the normal component of the relative displacement and can be associated with the opening mode, Mode I. The sliding mode, Mode II, generates ${}^{0}\mathbf{a}_1\mathbf{u}_{,\theta^i}$ components. The Mode III can be associated with the components ${}^{0}\mathbf{a}_3\mathbf{u}_{,\theta^i}$ and is zero in case of two-dimensional problems. By integrating equation (19) with the assumption of θ^2-independent stresses the two failure modes read

$$\begin{aligned} J_{\mathrm{I}} &= \tfrac{1}{2}\mathrm{h}\,(\tau_{\mathrm{A}}^{22}\ {}^{0}\mathbf{a}_2\mathbf{u}_{\mathrm{A},\theta^2} - \tau_{\mathrm{A}}^{12}\ {}^{0}\mathbf{a}_2\mathbf{u}_{\mathrm{A},\theta^1}) \\ J_{\mathrm{II}} &= \tfrac{1}{2}\mathrm{h}\,(-\tau_{\mathrm{A}}^{11}\ {}^{0}\mathbf{a}_1\mathbf{u}_{\mathrm{A},\theta^1} + \tfrac{1}{2}\tau_{\mathrm{B1}}^{11}\ {}^{0}\mathbf{a}_1\mathbf{u}_{\mathrm{B1},\theta^1} \\ &\quad + \tfrac{1}{2}\tau_{\mathrm{B2}}^{11}\ {}^{0}\mathbf{a}_1\mathbf{u}_{\mathrm{B2},\theta^1} + \tau_{\mathrm{A}}^{12}\ {}^{0}\mathbf{a}_1\mathbf{u}_{\mathrm{A},\theta^2})\,. \end{aligned} \tag{20}$$

The components ${}^{0}\mathbf{a}_1\mathbf{u}_{,\theta^1}$ and ${}^{0}\mathbf{a}_2\mathbf{u}_{,\theta^1}$ are dominated by the adherends stiffness and of small amount, if the ratio of adherends to adhesive stiffness is high. Finally, neglecting these components, a simple formulation can be found, which depends only on the adhesive thickness and the near tip stress and strain field of the region A

$$\begin{aligned} J_{\mathrm{I}} &= \tfrac{1}{2}\mathrm{h}\,(\tau_{\mathrm{A}}^{22}\,\varepsilon_{\mathrm{A}\,22}) \\ J_{\mathrm{II}} &= \tfrac{1}{2}\mathrm{h}\,(\tau_{\mathrm{A}}^{12}\,2\varepsilon_{\mathrm{A}12}) \\ &= \tfrac{1}{2}\mathrm{h}\,(\tau_{\mathrm{A}}^{12}\,\gamma_{\mathrm{A}12})\,. \end{aligned} \tag{21}$$

The applied stress and strain tensors in equation (21) allow a determination of *J* for two-dimensional problems with small deformations and finite rotations.

2.3 Finite element analysis

The following analysis demonstrates the application of the derived method. Therefore, two calculation examples of a DCB specimen are compared. Model A considers a usual finite element analysis taking into account the singular region at the crack tip with a fine mesh and inelastic material behavior. Model B does not contain the singularity and *J* is calculated by equation (21).

The finite element models are generated with the commercial program ABAQUS. Standard isoparametric 8-node elements CPS8R are used considering a plane stress state. Both analyses are performed in geometric linear way.

Figure 4 shows a loaded DCB specimen. All geometrical and physical input data are adapted to executed experiments. Each adherend

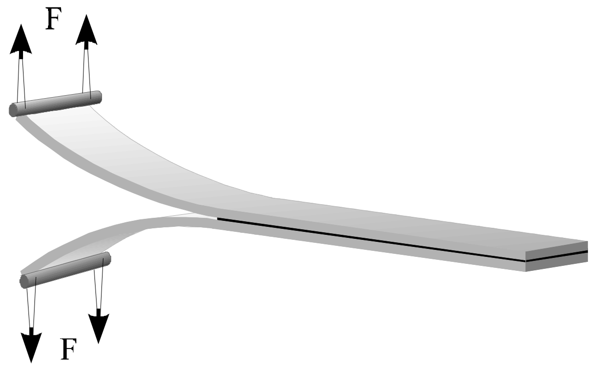

Figure 4: Double Cantilever Beam (DCB) specimen

is build up by 6 layers of the carbonfibre reinforced prepreg system 913C (Ciba Geigy) with a 0°-orientation to the θ^1-axis. A linear elastic orthotropic material behavior is applied to the models. The adherends are bonded with the structural adhesive-film Scotch Weld AF 163-2K (3M Company). The inelastic behavior of the adhesive in Model A is taken into account with a rate independent plasticity model with isotropic hardening. It should be noted, that in case of plastic behavior J can only be evaluated for monotonic loading and furthermore, J looses its meaning considering energy release theorems. In Model B a linear elastic behavior is adopted.

A part of the meshing of the two models in the deformed configuration is depicted in the figures 5 and 6. The dark-grey color represents the adhesive and the adherends are light-grey. Except for the crack region both meshes are nearly identical.

The mesh of Model A is idealized in accordance to standard fracture procedures of ABAQUS. Model A (figure 5) contains an intense mesh refinement with a circular focused mesh for the J-integral evaluation at the crack tip, at which the 8-node crack tip elements are collapsed. Their midside nodes are moved to the quarter point and the crack tip nodes are allowed to move independently, which creates a combined square root and 1/r singularity.

In Model B (figure 6) only a smooth mesh refinement is applied in θ^1-direction satisfying the non-singular strain and stress gradient. A linear variation of displacement is permitted in the θ^2-direction of the adhesive. In this case the three regions A, B1 and B2 do not interfere with each other, that means, the nodes at the crack tip boundary are allowed to move independently.

The DCB specimen is loaded at the ends of the debonded adherends according to figure 4. The analyses are performed with the maximum force of a single step cyclic loaded experiment, which can be classified as a fracture problem in the transition range from low to high cycle fatigue considering the crack growth onset (chapter 3).

The global deformation behavior can be characterized by the maximum deflections at the load introduction points. The maximum deflection of Model B is 0.8 ‰ lower than that of Model A. Both solutions are within the tolerance of the experimental measurement. The deviation of 0.8 ‰ can be explained with the appearance of inelastic deformations in Model A. Thus, both analyses compute identical global deformations applying a linear elastic

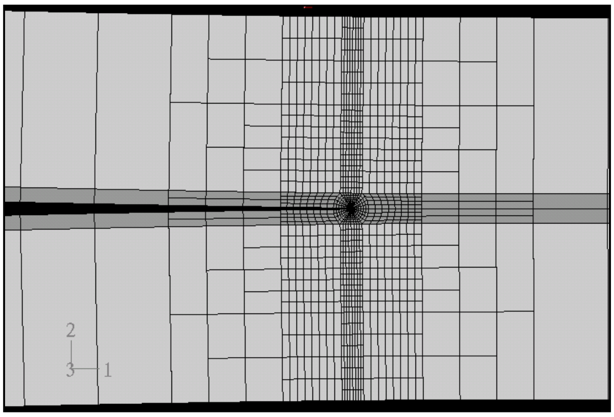

Figure 5: Finite element mesh of Model A

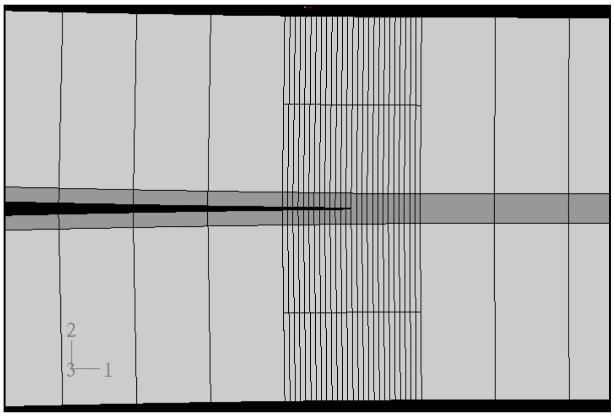

Figure 6: Finite element mesh of Model B

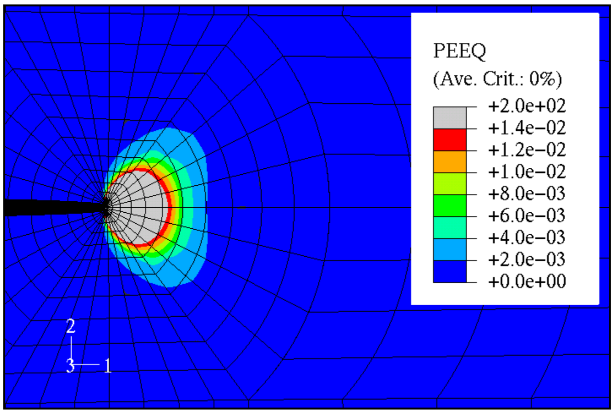

Figure 7: Equivalent plastic strain of the crack tip region (Model A)

approach in Model A.

Figure 7 shows the equivalent plastic strain distribution of Model A at the crack tip singularity caused by the peeling loading. The vertical size of the depicted detail in figure 6 coincides with the adhesive thickness. The characteristic size of the fracture process zone can be defined as the region, where non-proportional loading, large strains and other phenomena associated with fracture occur. It can be argued, that J can be used as a fracture criterion, if any event that occurs in the process zone is controlled by the deformation in the surrounding region. Thus, the process zone must be small compared to the region, which imposes the deformation of the singularity. In case of adhesively bonded joints the deformation in the adhesive is controlled by the rigid adherends and the process zone must be within the adhesive, which is valid for the considered analysis.

The peeling stress distribution of the crack tip region is depicted for both models in figure 8 and 9. The adhesive stress distribution of Model B only depends on the θ^1-coordinate caused by the linear shape function in θ^2-direction of the adhesive elements. The stress estimate at the crack tip is finite, contrary to a linear elastic solution of crack tip singularities. Comparing the analyses the stress distribution of Model A equals the approximate solution of Model B except of the singular crack tip zone. Applying equation (21) the approximate estimate of J = 0.596 N/mm for Model B is 1.3 % lower than the reference value J = 0.604 N/mm for Model A, which is calculated with a standard method of ABAQUS.

The results indicate the validity of the simplified method with acceptable accuracy in case of moderate loaded adhesively bonded joints. With increasing loads the plastic deformations affect the global deformation behavior and the assumptions of the theoretical investigations as well as the derivation of J are not valid anymore.

3 Experimental investigations

The investigations presented in chapter 2 are based on the existence of a sharp crack. Nevertheless, the theory can be applied to crack initiation problems considering the energetic conditions at the adhesive edges. Thus, the adhesive contains flaws and microcracks, which behave in a fracture mechanical way and which

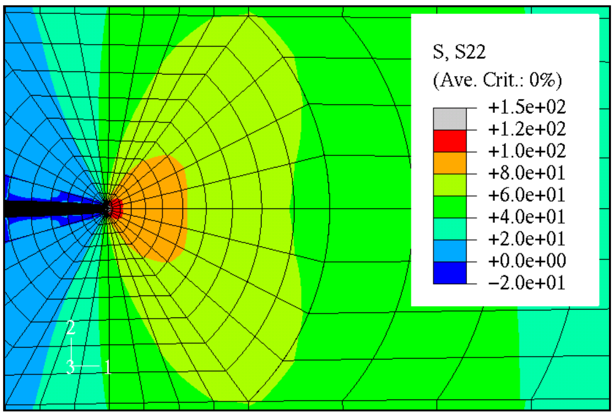

Figure 8: Peeling stress τ^{22} /(MPa) of the crack tip region (Model A)

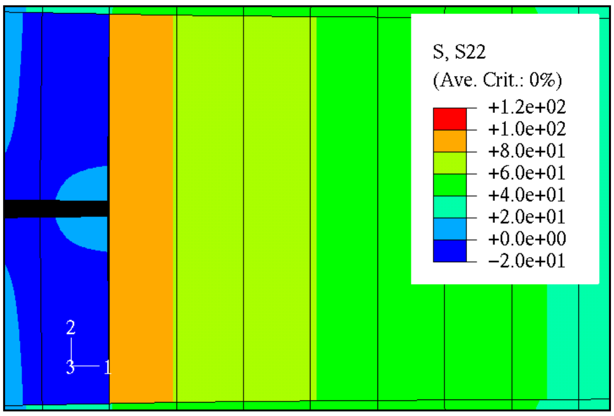

Figure 9: Peeling stress τ^{22} /(MPa) of the crack tip region (Model B)

contribute to the crack initiation at the adhesive edges. Fracture tests on DCB and Single-Lap Joint (SLJ) specimens (see figure 10) confirm this statement. The DCB specimens contain artificial debondings to enable the crack initiation investigations.

As mentioned above each adherend is made of 6 layers of the carbonfibre reinforced prepreg system 913C (Ciba Geigy) with a 0°-orientation to the θ^1-axis. The laminate has a nominal resin content of 40 % and was cured in an autoklave at 125 °C and a pressure of 700 kPa. The cured adherends were bonded with the structural adhesive-film Scotch Weld AF 163-2K (3M Company) with the same curing temperature and a pressure of 300 kPa. The DCB specimens were produced with a specimen width of 30 mm and 80 mm debond length. The SLJ specimens were manufactured with a width of 25 mm and the two different joint lengths 20 mm and 30 mm. In order to realize a multifariousness of geometric variations four adhesive thicknesses were maintained by metal shims of 0.05 mm, 0.15 mm, 0.25 mm and 0.35 mm inserted between the adherends before bonding.

The single step fatigue tests of the DCB

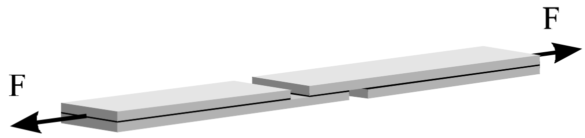

Figure 10: Single Lap Joint (SLJ) specimen

and SLJ specimens were executed in a servohydraulic test machine and were loaded harmonically with a load ratio of

$$R = \frac{F_{min}}{F_{max}} = 0 \quad . \qquad (22)$$

The frequency was adjusted to the displacement amplitude in order to realize a constant average speed of load application.

At certain load cycles the applied loads and the displacements were monitored continuously. The current crack length was determined by the compliance method, i. e. the crack length was obtained by the measured compliance of the body. The relation between the debond length and the counted fatigue cycles provided the debond growth rate. At the beginning of the fatigue tests most experiments showed a plateau with negligible growth rates, considering the debond length plotted against cycles. The end of

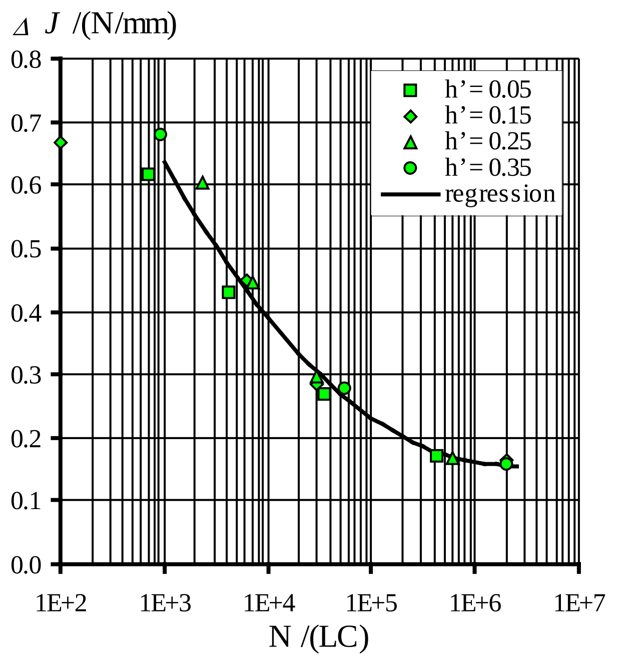

Figure 11: Crack initiation of cyclic loaded DCB specimens ($\Delta J_{II} \approx 0$), shim thickness - h'

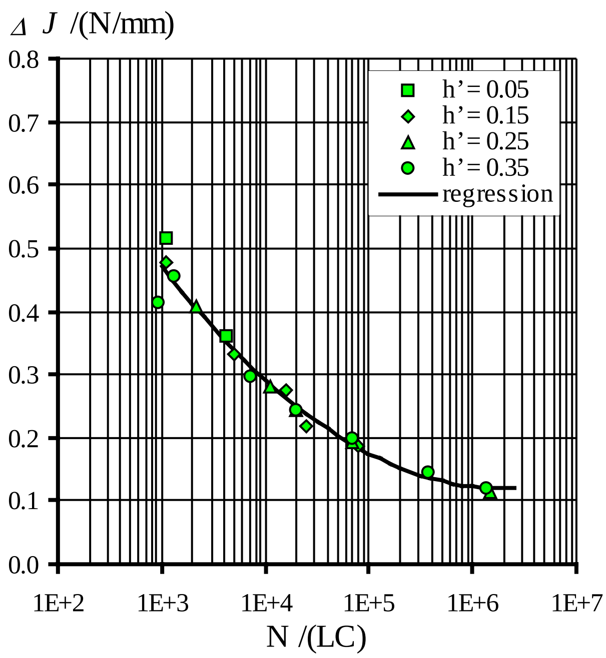

Figure 12: Crack initiation of cyclic loaded SLJ specimens (ΔJ_{I} / $\Delta J_{II} \approx 0.65$), shim thickness - h'

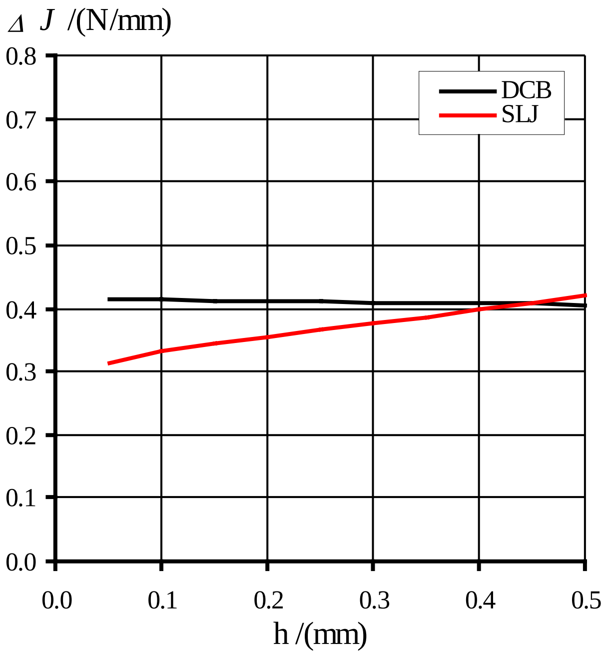

Figure 13: Adhesive thickness dependency of DCB specimens (ΔF = 55 N) and SLJ specimens (ΔF = 5 kN; ℓ = 20 mm)

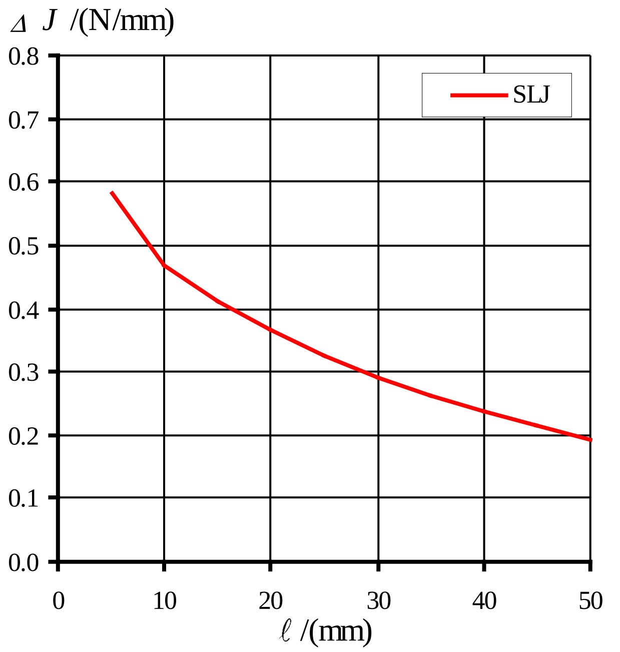

Figure 14: Joint length dependency of SLJ specimens (ΔF = 5 kN; d = 0.25 mm)

this plateau indicates the crack growth onset respectively the crack initiation.

Crack initiation data obtained from the DCB and SLJ fatigue tests are shown in the figures 11 and 12. An equation of the form

$$\Delta J = c_1 \ell g(N_{ci}) + c_2 (\ell g(N_{ci}))^2 + c_3 \qquad (23)$$

was fitted to the data in both figures by using a least-squares regression analysis. ΔJ is the J-amplitude obtained by equation (21) with geometric nonlinear analyses, and N_{ci} is the number of cycles at crack initiation. Both regressions (figure 11 and 12) have a similar behavior and a good correlation to the test data. Each figure shows data from specimens with different bond line thicknesses. Furthermore, results of the two joint lengths 20 mm and 30 mm are depicted in figure 12. Considering the variations of geometry the data are statistically scattered, and no systematic deviations can be recognized. This suggests that crack initiation is a function of ΔJ and that the applied method is valid. Comparing the figures 11 and 12 the SLJ specimens with a mixed mode ratio of ΔJ_I / ΔJ_{II} ≈ 0.65 behave more critically against crack initiation. This indicates a functional relation of the mode ratio on the crack growth onset. In the logarithmic plotting the regressions are practically speaking linear up to a cycle number of 1E+5. Estimates of no-growth thresholds are ΔJ_{th} ≈ 0.15 N/mm for the DCB specimens and ΔJ_{th} ≈ 0.11 N/mm for the SLJ specimens. This is about one tenth of the static fracture toughness.

Some essentials to the fracture characterization of fatigue loaded adhesive bondings can be noticed considering the influence of the main geometrical dimensions on the fracture parameter ΔJ. The crack initiation does not depend on the adhesive thickness in case of mode I loaded DCB specimens, whereas an increasing thickness of mixed mode loaded SLJ specimens results in growing ΔJ-values (see figure 13). Doubling the adhesive thickness from 0.2 mm to 0.4 mm the crack initiation life is halved for example. The dependence of the joint length ℓ on ΔJ illustrated in figure 14 is not of general validity taking into account the boundary conditions of the adherends. Nevertheless, the SLJ specimens show a significant deterioration of the debond resistance for joint lengths below 10 mm. This is caused by the interference of the two free edge effects of the bonding, where the spatial extent of the free edge effects is a linear function of the adhesive thickness.

Conclusion

A calculation method was developed for a simple determination of the path independent J-integral in case of adhesively bonded joints. The investigations are based on a method, which bypasses the detailed determination of the strain singularity and the inelastic material behavior at the crack tip. Thus, the J-integral can be obtained with the results of a simple continuum mechanics analysis reducing the expenditure of the structural modeling.

Acceptable accuracy was obtained in case of moderate loaded adhesively bonded joints in comparison with standard methods including the effects of the crack tip singularity and inelastic material behavior. This enables the application of the method to the fracture characterization of fatigue loaded adhesive bondings.

Single step fatigue experiments on DCB and SLJ specimens show the validity of the theoretical investigations. The crack initiation data are statistically scattered and no systematic deviations can be recognized considering the multifariousness of the tested geometric variations. This suggests that crack initiation is a function of ΔJ and the mode ratio $\Delta J_{\mathrm{I}} / \Delta J_{\mathrm{II}}$.

References

[1] Rice J R. A path independent integral and the approximate analysis of strain concentration by notches and cracks. *Journal of Applied Mechanics*, Vol. 35, pp 379-386, 1968.

[2] Volkersen O. Die Nietkraftverteilung in zugbeanspruchten Nietverbindungen mit konstanten Laschenquerschnitten. *Luftfahrtforschung*, Vol. 15, pp 41-47, 1938.

[3] Goland M and Reissner E. Stresses in cemented joints. *Journal of Applied Mechanics*, Vol. 11, pp A17-A27, 1944.

[4] Hart-Smith L J. Adhesive bonded single-lap joints. *NASA*, CR-112236, 1973.

[5] Matthews F L. *Joining fibre-reinforced plastics*. Elsevier Applied Science Publishers LTD London and New York, 1987.

[6] Kanninen M F and Popelar C H. *Advanced fracture mechanics*. Oxford University press New York, 1985.

[7] Fernlund G, Lanting H and Spelt J K. Mixed mode II-mode III fracture of adhesive joints. *Journal of Composites Technology & Research*, Vol. 17, No. 4, pp 317-330, 1995.

[8] Fraisse P and Schmit F. Use of J-integral as fracture parameter in simplified analysis of bonded joints. *International Journal of Fracture*, Vol. 63, No. 1, pp 59-73, 1993.

[9] Eschenauer H and Schnell W. *Elastizitätstheorie I: Grundlagen Scheiben und Platten*. Bibliographisches Institut, B.I.-Wissenschaftsverlag Mannheim, Wien and Zürrich, 1981.

[10] Rybicki E F and Kanninen M F. A finite element calculation of stress intensity factors by modified crack closure technique. *Engineering Fracture Mechanics*, Vol. 9, pp 931-938, 1977.